Journal of Applied Electrochemistry (2022) 52:103–114
https://doi.org/10.1007/s10800-021-01621-6

RESEARCH ARTICLE

Microwave-assisted synthesis of ZnO decorated acid functionalized carbon nanotubes with improved specific capacitance

Sohini Chakraborty[1] · Remya Simon[1] · R. Antonia Trisha Zac[1] · Vadakkekara Anoop[1] · N. L. Mary[1]

Received: 22 February 2021 / Accepted: 9 August 2021 / Published online: 10 October 2021

Abstract

The fabrication and testing of new materials for energy storage applications is slowly gaining impetus amidst the constantly developing technological sector. Carbon-based materials have been extensively used for their high surface area, conductivity and good mechanical properties. Here, acid functionalized carbon nanotubes and its ZnO composite have been prepared using a facile microwave assisted technique and their electrochemical performances have been compared. The samples have been characterised using spectral techniques such as UV–Visible, FTIR and Raman spectroscopy. Their surface morphology has been studied using Scanning electron microscopy. X-ray diffraction analysis has been performed on the samples to further characterise the synthesised nanomaterials. Their electrochemical properties were investigated using cyclic voltammetry, chronopotentiometry and AC impedance techniques. The samples exhibit enhanced specific capacitance and good cycling stability. A high value of specific capacitance was achieved for CNT-COOH/ZnO thereby reinforcing the improvement of electrochemical characteristics of acid functionalized carbon nanotubes through composite formation.

✉ N. L. Mary
maryterrysmc@gmail.com

[1] Department of Chemistry, Stella Maris College (Autonomous), University of Madras, Chennai 600086, India

Graphic abstract

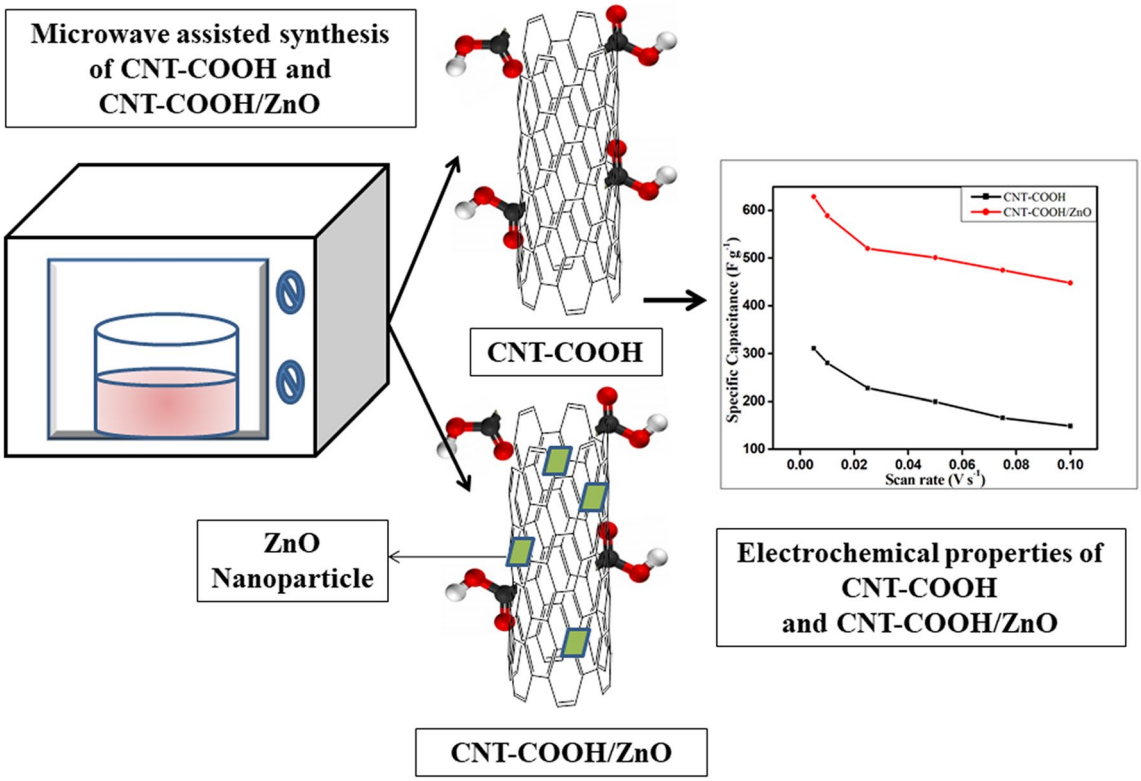

Keywords Carbon nanotubes · Microwave synthesis · Zinc oxide · Functionalisation · Specific capacitance

1 Introduction

The present industrial scenario relies greatly on the proficient storage and utilisation of energy. To enable these demands, energy storage devices have been extensively studied in order to develop high performance novel systems [1–4]. Also, the rapid depletion of the non-renewable sources of energy leads us to shift our focus on harvesting and storing the energy from the available renewable sources [5, 6]. Supercapacitors have emerged as devices which can store and deliver energy efficiently thereby enabling the concept of sustainable energy storage [7]. Tremendous emphasis has been laid on modifying the existing materials and discovering new materials for energy storage applications. Electrical double layer capacitors depends mainly on the high surface area of the carbonaceous material while pseudocapacitors such as conducting polymers and metal oxides rely on redox reactions for energy storage [8–10]. The proper combination of both these mechanisms ensures the fabrication of highly stable electrochemical supercapacitors.

Carbon nanotubes (CNT) have been used to a great extent as electrode materials for supercapacitors due to its high surface area, charge transport ability, high conductivity and mesoporous nature [11]. Efforts have been made to functionalise the molecular backbone of these nanotubes to enhance its properties [12, 13]. The specific capacitance is expected to improve greatly with functionalisation. Strong oxidation of CNT has been reported to greatly improve its capacitance [14]. Functionalisation also provides the advantage of introducing polar groups on the surface of CNT which can increase its hydrophilicity thereby imparting high values of specific capacitance in aqueous electrolytes [15, 16]. In addition to this, it also eases the formation of composites with metal oxides through electrostatic interactions [17]. Hybrid electrodes of functionalized CNT and metal oxides employ dual mechanisms of pseudocapacitance and double layer capacitance to allow the ions to diffuse easily throughout the network.

Amongst the metal oxides, ruthenium oxide has been widely used for supercapacitor applications [18]. However, due to its high cost and low abundance, alternative materials have been investigated for these applications. Zinc oxide with its good electrical and optical properties has been used as an alternative to develop these devices [19, 20]. High specific capacitance values can be obtained

when they are incorporated into the interconnected network of CNT. The mechanical property which is an important parameter for device fabrication also improves with the formation of composites [21, 22]. Various other supercapacitor electrodes have also been developed using the combination of a metal oxide and carbonaceous materials. Zhang et al. has reported the synthesis of nickel molybdate and reduced graphene oxide/multiwalled CNT nanocomposites using the solvothermal method. $NiMoO_4$/rGO and $NiMoO_4$/MWCNTs electrode materials exhibited altered morphology and higher capacitive properties with capacitance retention of 66.7 % for $NiMoO_4$/MWCNTs even after 1000 cycles [23]. $NiMoO_4$ has also been modified with $MnMoO_4$, $ZnMoO_4$ and $CoMoO_4$ to prepare electrode materials with distinctive morphologies to obtain high capacitance retention and specific capacitance [24]. Ammonium nickel-cobalt phosphate (NNCP) which is a versatile binary transition metal compound often used as an inorganic catalyst has also been explored for its electrochemical properties. Composites of NNCP with metal oxides such as CuO, MnO_2 and Co_3O_4 exhibited very high specific capacitances. NNCP/MnO_2 with its unique flower-like interfacial characteristic displayed the highest specific capacitance and enhanced rate capability [25]. All these reports emphasize that composite formation with other transition metal oxides and carbonaceous materials greatly influence the electrochemical behaviour of the fabricated electrodes.

In the present work, CNT has been acid functionalized (CNT-COOH) and CNT-COOH/ZnO composite has been synthesised. The effective functionalisation and incorporation of ZnO has been studied through characterisation techniques. The electrochemical properties of these two materials have been compared and the effect of composite formation on the specific capacitance has been studied in details. These results signify that on combining the double layer capacitance of CNT and the pseudocapacitance of ZnO through effective composite formation, novel materials with high electrochemical performance can be developed.

2 Materials and methods

2.1 Materials used

Multiwalled carbon nanotubes (MWCNT, 110–170 nm diameter and 5–9 µm length), polytetrafluoroethylene powder and Zinc nitrate were procured from Sigma Aldrich and were used without further purification. All the solutions were prepared using millipore water.

2.2 Synthesis of acid functionalized carbon nanotubes (CNT-COOH)

MWCNT was acid functionalized using a microwave assisted technique as per a reported procedure [26]. To 0.1 g of MWCNT, 5 ml of concentrated nitric acid was added as an oxidant and the entire solution was kept in a microwave oven at an operating power of 600 W and a temperature of 160 °C for 30 min. Subsequent oxidation of MWCNT took place after the stipulated time period. The obtained product was filtered and dried at 50 °C in a hot air oven for an hour. Scheme 1 represents the preparation of CNT-COOH.

2.3 Synthesis of ZnO and acid functionalized carbon nanotubes composites (CNT-COOH/ZnO)

ZnO and MWCNT-COOH composite was prepared by the co-precipitation method [27]. CNT-COOH prepared by the above method was dissolved in millipore water and sonicated for an hour. 0.5 g of Zinc Nitrate was dissolved in 20 ml of deionised water and was added dropwise to the sonicated CNT-COOH with constant stirring at a temperature of 50 °C. 1 M NaOH was added to the above mixture and the pH level was maintained at 10 in order to precipitate $Zn(OH)_2$ and stirring was continued for an hour. The mixture was kept aside and the precipitate was allowed to settle. It was then filtered and washed with deionised water, dried at 70 °C for an hour and calcined at 350 °C to obtain CNT-COOH/ZnO. Scheme 2 represents the preparation of CNT-COOH/ZnO.

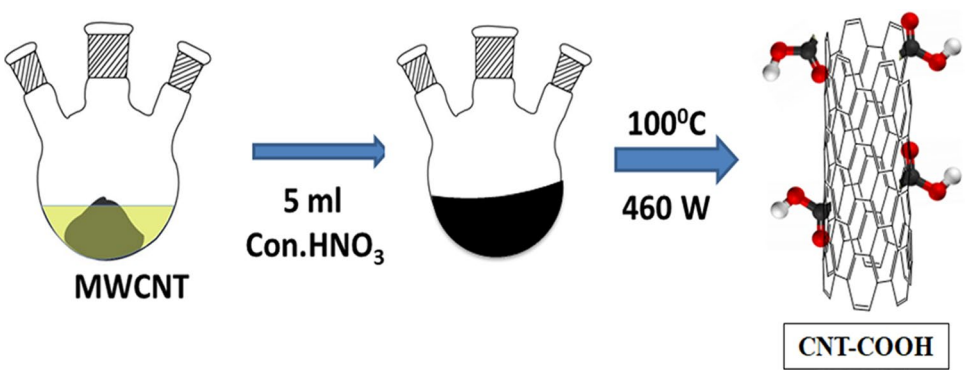

Scheme 1 Schematic representation of synthesis of acid functionalized carbon nanotubes (CNT-COOH)

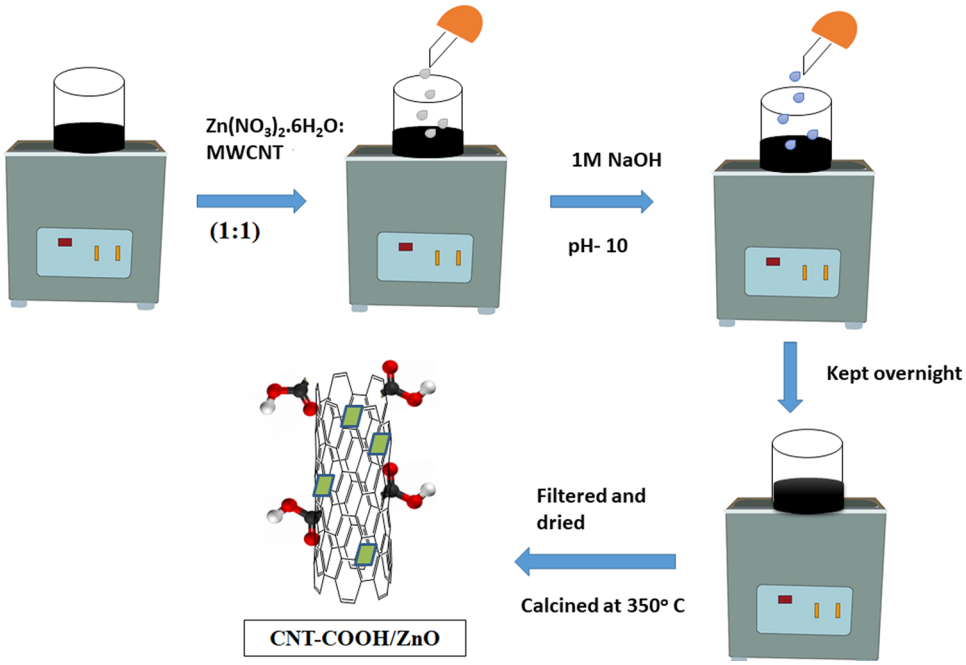

Scheme 2 Schematic representation of synthesis of composite of ZnO and acid functionalized carbon nanotube (CNT-COOH/ZnO)

2.4 Characterization techniques

The UV–Visible spectra of the samples were recorded in the wavelength range of 200–800 nm using a Jasco V-750 solid UV–Visible spectrometer. The FTIR spectra were obtained using a Bruker ATR-FTIR Model Alpha-T in the range of 400–4500 cm^{-1} at a scan rate of 24 per second. X-ray diffraction analysis of the samples was performed using a Bruker D8 Advance diffractometer. The Raman frequencies were studied using Bruker RFS 27 FT-Raman Spectrometer at a scan range of 50–4000 cm^{-1} with a resolution of 2 cm^{-1}. The surface morphology was studied using the FEI Quanta FEG 200 - High Resolution Scanning Electron Microscope (HR-SEM) and the electrochemical measurements were carried out using a CH 608 E Electrochemical Workstation (CH Instruments, USA).

2.5 Electrochemical measurements

The electrochemical studies were performed using a CH 608 E electrochemical workstation. A three electrode system comprising of a modified glassy carbon electrode as the working electrode, Ag/AgCl as the reference electrode and Pt wire as the counter electrode was used to perform the electrochemical studies. The studies were carried out at room temperature (25 °C ± 1) and 1 M H_2SO_4 was used as the electrolyte. The working electrode was coated with the samples using the drop casting technique. A dispersion of 1 mg mL^{-1} of the samples was prepared by ultrasonication using Polytetrafluoroethylene (PTFE) as the binder and ethanol as the solvent. 3 µL (0.003 mg) of the sample was then coated on the polished surface of the glassy carbon electrode and it was used as the working electrode. The cyclic voltammograms were recorded at the potential range of − 0.2 to 0.4 V at a scan rate of 5–100 mV s^{-1}, the galvanostatic charge-discharge measurements were performed at the current densities of 1 Ag^{-1} and 2 Ag^{-1} and the impedance measurements were carried out at the frequency range of 10^{-2} to 10^{5} Hz.

3 Results and discussion

3.1 UV–Visible spectroscopy

Figure 1 shows the UV–Visible spectra of CNT-COOH and CNT-COOH/ZnO. A ad absorption band is observed at 200–250 nm for both the samples. This can be attributed to the π-π* transition characteristic of MWCNTs [28]. An additional peak at 400–450 nm is observed in the spectra of CNT-COOH/ZnO which indicates the efficient incorporation of ZnO nanoparticles into the matrix of acid functionalized MWCNT. A red shift is observed in this case which can be ascribed to the interaction between the carbonyl oxygen of the carboxyl group and the ZnO nanoparticles [29]. This interaction results in a change in polarisability of the environment leading to the shift in wavelength [30]. The peak intensity for CNT-COOH/ZnO is depicted to be slightly less than that of CNT-COOH. The inclusion of ZnO nanoparticles into the matrix of acid functionalized MWCNT results in interactions with the π electrons of MWCNT which in

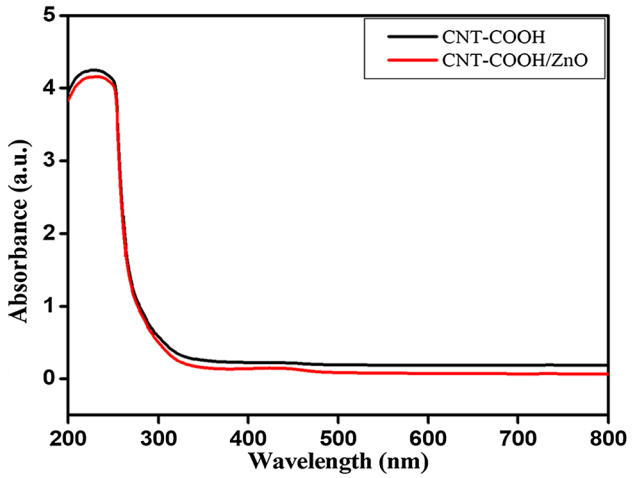

Fig. 1 UV–Visible spectra of CNT/COOH and CNT-COOH/ZnO

turn influences the extended conjugation system resulting in inappreciably lower absorbance values.

3.2 FTIR spectroscopy

The FTIR spectra of CNT-COOH and CNT-COOH/ZnO are depicted in Fig. 2. In Fig. 2a, a highly intense absorption peak is observed at 3409 cm^{-1} which is due to the stretching vibration of the hydroxyl functional group. The peak at 1744 cm^{-1} can be ascribed to the carbonyl stretching vibration of the carboxyl group and the peak at 1638 cm^{-1} is due to the C–O stretch from the quinine ring structure formed during the oxidation of MWCNT. The broad peak at 1253 cm^{-1} can be attributed to the C–C stretching vibration [31].

Figure 2b represents the FTIR spectra of CNT-COOH/ZnO. On addition of ZnO to the matrix of functionalized CNT, polar bonds are formed between ZnO and the oxygen containing groups of functionalized CNT which results in a shift in absorption to higher wave numbers. Thus the C=O stretching frequency shifts from 1638 to 1646 cm^{-1} due to the presence of interaction between the carbonyl oxygen and the metal oxide. The O–H vibrational frequency appears at 3423 cm^{-1}. In addition to all the above absorption bands, an additional band is observed between 400 and 500 cm^{-1} which can be attributed to the stretching vibration of Zn-O [32].

3.3 X-ray diffraction analysis

Figure 3 shows the X-ray diffraction plots of the samples. They appear to be highly crystalline in nature with the presence of sharp diffraction peaks. The diffractogram of CNT-COOH (Fig. 3a) exhibits two intense peaks at a $2\theta = 26.672°$ and 42.127° which can be attributed to the (002) and (100) diffraction planes characteristic to acid functionalized MWCNT [33]. The peaks for functionalized MWCNT is observed along with peaks at 31.26°, 33.5°, 36.4°, 47.8°, 54.2°, 58.5° corresponding to (010), (002), (011), (012), (110) and (013) diffraction planes which can be correlated to the hexagonal wurtzite structure of the ZnO nanoparticles which are consistent with the JCPDS data number 36–1451 for CNT-COOH/ZnO (Fig. 3b) [34].

3.4 Raman spectroscopy

Figure 4 illustrates the Raman spectra of the samples. The spectra is characterised by two main modes of vibrations, G and D. The D band occurs at 1303 cm^{-1} and 1397 cm^{-1} while the G band occurs at 1613 cm^{-1} and 1623 cm^{-1} for CNT-COOH and CNT-COOH/ZnO, respectively. D band is usually related to the non-crystalline sp^3 hybridised carbon while G band corresponds to the stretching modes of sp^2 carbon atoms of graphitic materials. Functionalisation of

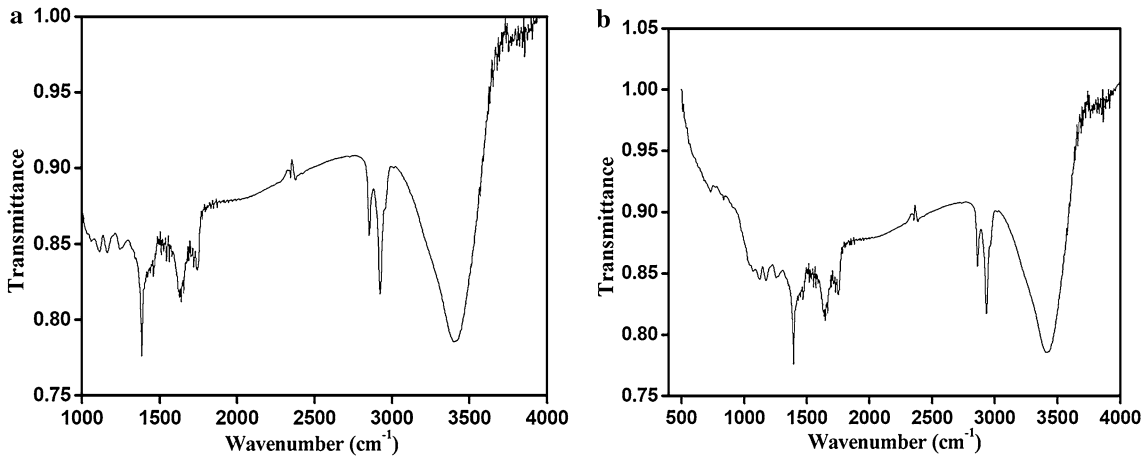

Fig. 2 FTIR spectra of **a** CNT-COOH and **b** CNT-COOH/ZnO

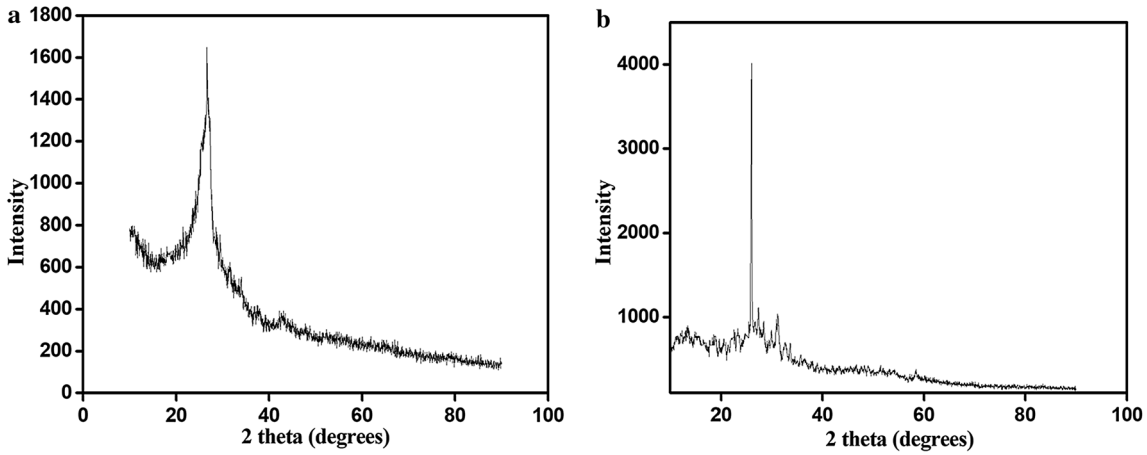

Fig. 3 X-Ray diffraction studies of **a** CNT-COOH and **b** CNT-COOH/ZnO

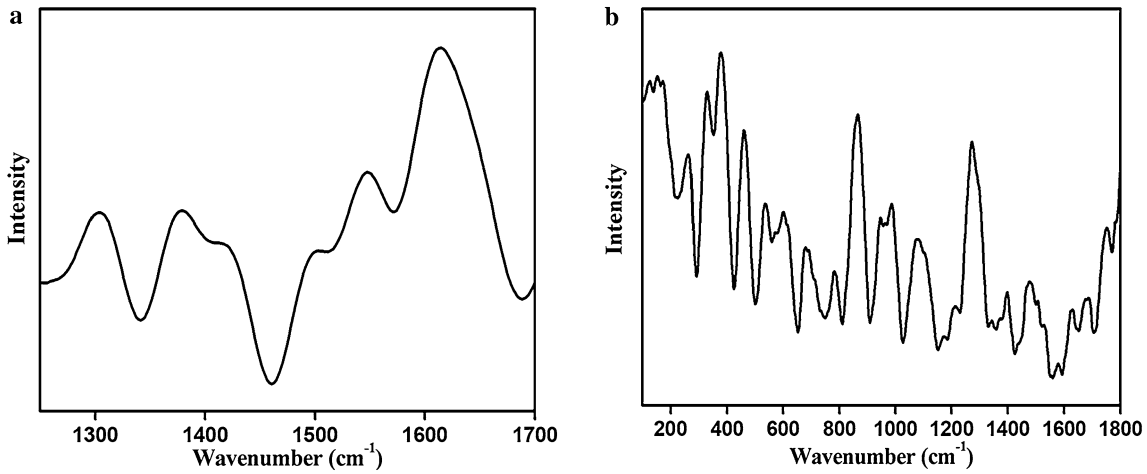

Fig. 4 Raman spectra of **a** CNT-COOH and **b** CNT-COOH/ZnO

CNT results in the loss of aromaticity caused by defects induced by the oxygen atoms from the carboxyl functionalities introduced in the structure. These groups can bind with the carbon atoms on the exterior walls and change the hybridisation state from sp^2 to sp^3. These changes can be observed by calculating the ratio of the intensities of the D band and the G band (I_D/I_G). This ratio increases with the number of disordered carbon atoms. The ratio is 0.64 for CNT-COOH and it increases to 0.85 for CNT-COOH/ZnO [35].

In Fig. 4b, the basic phonon modes of hexagonal ZnO has been obtained at 121, 378, 462 and 595 cm^{-1} which represents the E_{2L}, A_1, E_{2H} and A_1/E_1 symmetry, respectively. The second order phonon mode has been observed at 149 cm^{-1} which can be assigned to $2E_{2L}$. The multi phonon scattering modes are observed at 328, 604, 681 and 1078 cm^{-1}. The acoustic combination of A_1 and E_2 is observed at 1276 cm^{-1} [36].

3.5 Scanning electron microscopy

The SEM micrographs in Fig. 5 shows the surface morphology of CNT-COOH and CNT-COOH/ZnO. The nanotubes form a well-interconnected network as is observed in Fig. 5a. The interconnected conductive framework on nanotubes is expected to greatly influence its electrochemical properties [37]. ZnO nanoparticles are exhibited to be distributed on

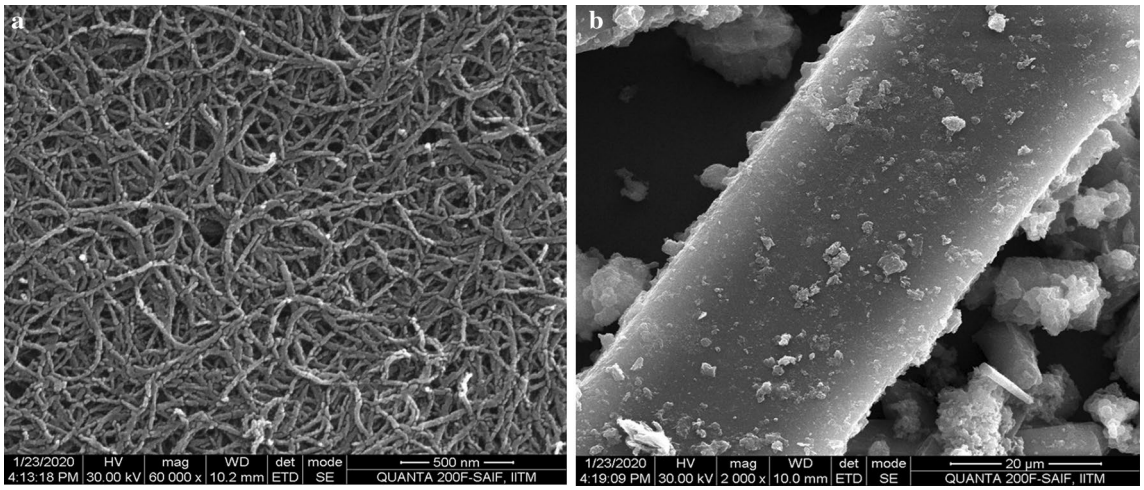

Fig. 5 SEM micrographs of **a** CNT-COOH **b** CNT-COOH/ZnO

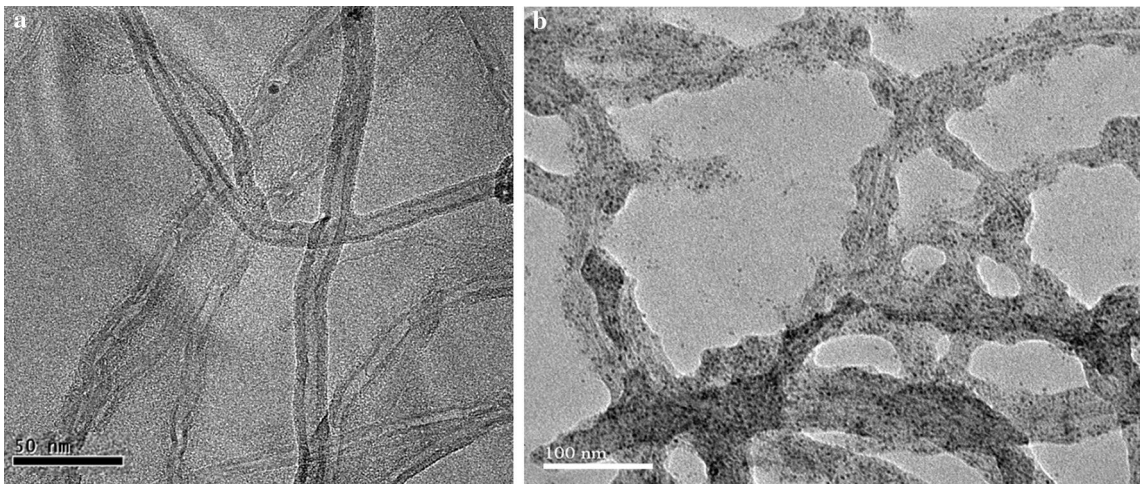

Fig. 6 TEM image of **a** CNT-COOH and **b** CNT-COOH/ZnO

the surface of the nanotubes in a nanoflake arrangement as observed in Fig. 5b.

3.6 Transmission electron microscopy

Figure 6 shows the TEM image of CNT-COOH and CNT-COOH/ZnO. The nanotubes in Fig. 6a are observed to form interconnected channels and its fracture surface is found to be smooth. The nanoflakes of ZnO can be observed to be distributed almost uniformly all along the length and breadth of the nanotubes of CNT-COOH/ZnO in Fig. 6b. The proficient attachment of the ZnO onto the walls of the nanotubes results in the formation of an interface which is beneficial in improving the overall capacitive properties of the nanocomposite [38, 39].

3.7 BET analysis

BET is an efficient technique for determining the porosity of an amorphous microporous material. It helps in identifying the amount of surface area that is available for physical adsorption and is very helpful in precisely characterising the physical surface of a material. The BET isotherms of the samples are depicted in Fig. 7. The specific surface area of CNT-COOH/ZnO and CNT-COOH is found to be 28.55 $m^2\ g^{-1}$ and 18.68 $m^2\ g^{-1}$, respectively. The acid treatment followed by subsequent introduction of carboxyl groups has been reported to reduce the surface area to a great extent as it blocks the entry of the adsorbed gas [40–43]. The increase in surface area of CNT-COOH/ZnO can be attributed to the synergistic effect of CNT and ZnO. CNT-COOH and

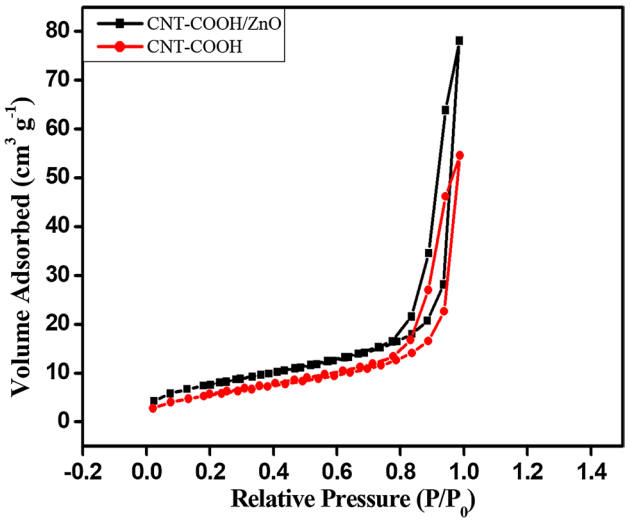

Fig. 7 BET isotherm of CNT-COOH and CNT-COOH/ZnO

CNT-COOH/ZnO exhibit a type IV isotherm with a hysteresis loop in the P/P_0 range of 0.8–1.0 and 0.7–1.0, respectively [44]. This indicates the mesoporous behaviour of the synthesised samples.

3.8 Electrochemical studies

The applications using the cyclic voltammetry and galvanostatic charge-discharge techniques. Figure 8 represents the cyclic voltammograms of CNT-COOH and CNT-COOH/ZnO. The CV curves in Fig. 8a are displayed to have a quasi-rectangular nature along with the presence of redox peaks. The acid functionalisation of MWCNT results in the presence of surface functional groups which render psuedocapacitance to the material. It has been reported that the presence of oxygen containing functional groups increases the surface wettability of CNTs making them more susceptible towards the physisorption of electrolyte ions which in turn enhances the ionic conductivity at the electrode-electrolyte interface [45]. In the case of CNT-COOH/ZnO (Fig. 8b), a more rectangular shaped loop is observed and the current response is also much higher than that of CNT-COOH indicating a more efficient capacitive behaviour. The humps in the voltammogram can be attributed to the redox-active nature of ZnO nanoparticles [46]. The combined effects of the electrical double layer capacitance of acid functionalized CNT and the psuedocapacitance of ZnO greatly influences the capacitive properties of the material.

To understand more effectively the enhanced specific capacitance of CNT-COOH/ZnO over CNT-COOH, the voltammograms have been compared at 5 mV s^{-1} and is represented in Fig. 9.

The specific capacitance of the samples has been calculated from CV using the formula:

$$Cv = \frac{\int_{v1}^{v2} idV}{V \times m \times (V2 - V1)}$$

Where i = instantaneous current (A), m = mass of electrode (g), V = potential scan rate (V s^{-1}), $V1$ = high potential of CV (V), $V2$ = low potential of CV (V) and Cv is the specific capacitance (F g^{-1}).

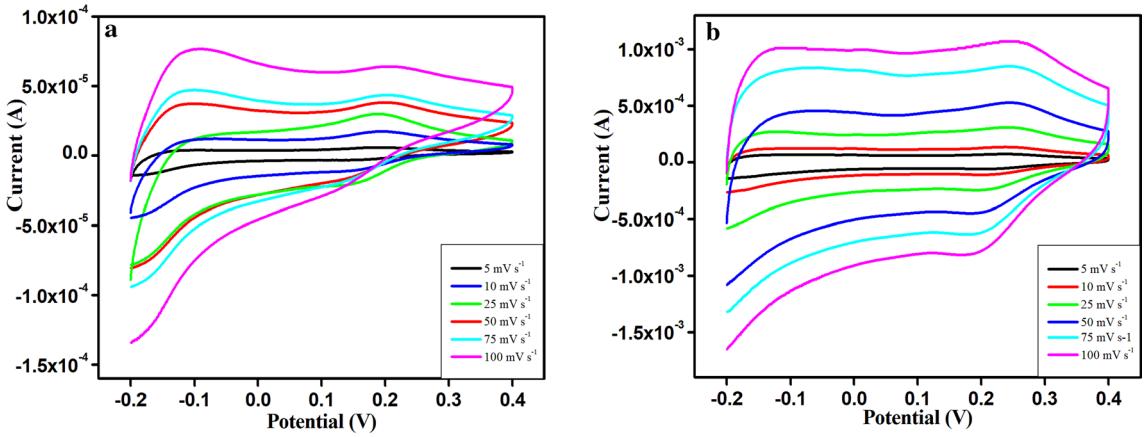

Fig. 8 Cyclic voltammograms of **a** CNT-COOH and **b** CNT-COOH/ZnO

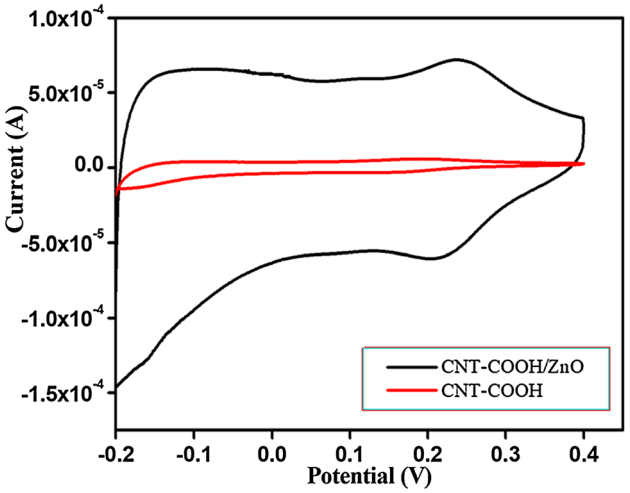

Fig. 9 Comparison of CV of CNT-COOH/ZnO and CNT-COOH at 5 mV s^{-1}

Table 1 Specific capacitance of CNT-COOH and CNT-COOH/ZnO at different scan rates

SL.No.	Sample code	Scan rate (mV s^{-1})	Specific capacitance (F g^{-1})
1.	CNT-COOH	5	311.1
		10	280.55
		25	227.77
		50	199.25
		75	165.55
		100	148.55
2.	CNT-COOH/ZnO	5	628.88
		10	588.88
		25	520
		50	500.74
		75	474.44
		100	447.77

The plot of specific capacitance versus scan rate has been represented in Fig. 10. A specific capacitance of 311.11 F g^{-1} and 628.88 F g^{-1} has been observed for CNT-COOH and CNT-COOH/ZnO, respectively. These values indicate a significant enhancement of specific capacitance for the composite of CNT-COOH with ZnO. The values of specific capacitance at different scan rates are tabulated in Table 1.

Figure 11 shows the chronopotentiometric response of the samples. The shape of the curves can be observed to be nearly triangular indicating good capacitive behaviour of the samples [47].

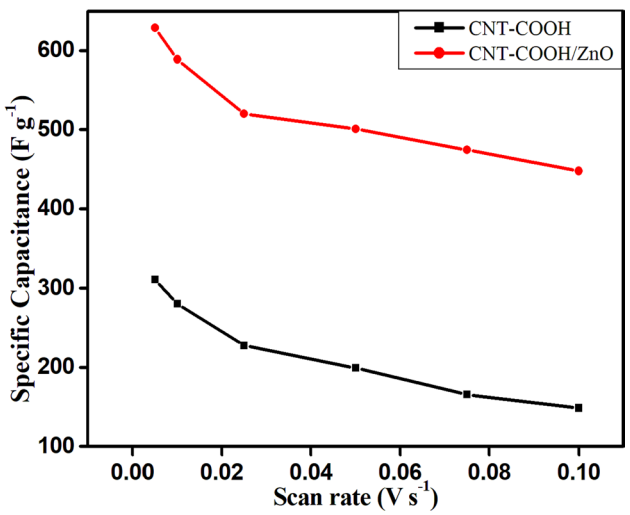

Fig. 10 Plot of specific capacitance versus scan rate of CNT-COOH and CNT-COOH/ZnO

The specific capacitance can be calculated using the formula below:

$$C_{sp} = \frac{i\Delta t}{m\Delta V}$$

Where *C*sp = specific capacitance (F g^{-1}), i = instantaneous current (A), Δt = discharge time (s), m = mass of electrode (g) and ΔV = potential window (V).

The specific capacitances of CNT-COOH were found out to be 360.25 F g^{-1} and 232.45 F g^{-1} at 1 A g^{-1} and 2 A g^{-1}, respectively. For CNT-COOH/ZnO, the specific capacitances are 612.2 F g^{-1} and 454.5 F g^{-1} at the current densities of 1 A g^{-1} and 2 A g^{-1}, respectively.

From the values of specific capacitance, it can be inferred that these materials serve as efficient platforms for electrochemical applications. The specific capacitance values are observed to be highly enhanced on incorporation of ZnO nanoparticles to CNT-COOH. This can be attributed to the combined pseudocapacitive properties of ZnO and the double layer capacitance of CNT in CNT-COOH/ZnO.

The cycling stability of the samples was evaluated at the current density of 1 A g^{-1} for 1000 segments (Fig. 12). The samples show good cycling stability with maximum capacitance retention.

The electrochemical impedance spectra of the samples are represented in Fig. 13. The samples exhibit a depressed semicircle at the high frequency region and a vertical spike

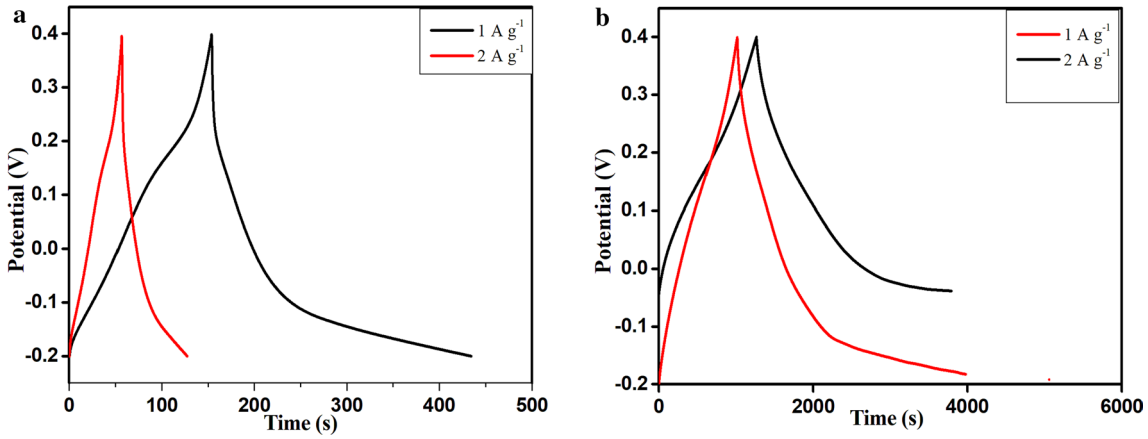

Fig. 11 Charge-discharge curves of **a** CNT-COOH and **b** CNT-COOH/ZnO

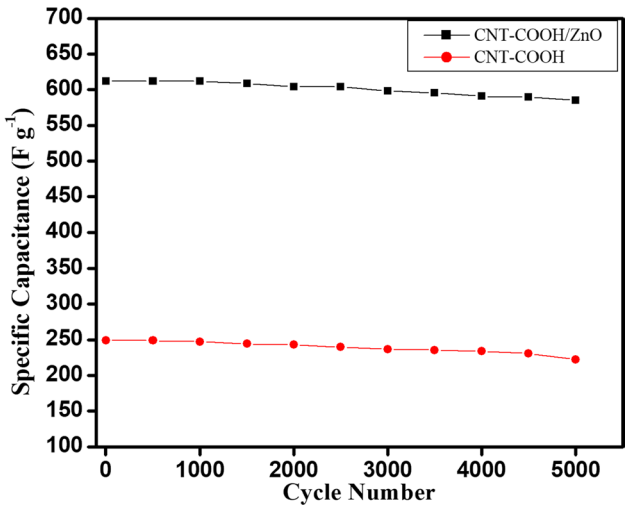

Fig. 12 Cycling stability of CNT-COOH/ZnO and CNT-COOH

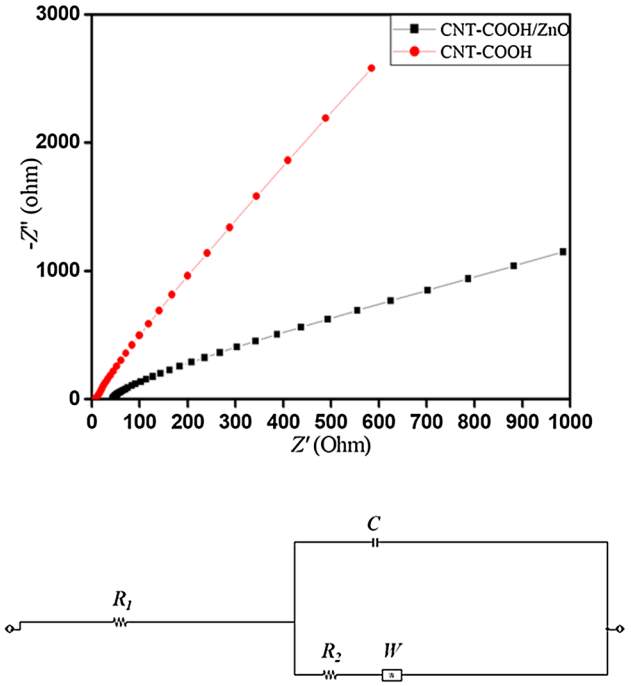

Fig. 13 Impedance spectra and the equivalent Randles circuit of CNT-COOH and CNT-COOH/ZnO

at the low frequency region [48]. The Nyquist plot obtained was fitted into the Randle's equivalent circuit using the ZsimpWin software (Version 3.21) and the values obtained are tabulated in Table 2.

*R*s is the solution resistance, *R*ct is the charge transfer resistance, *C* is the double layer capacitance and *W* is the Warburg resistance. From the table it can be concluded that the capacitance is greater for CNT-COOH/ZnO when compared to CNT-COOH indicating better electrochemical performance of the sample. The charge transfer resistance can also be observed to be very low for CNT-COOH/ZnO which implies that it has greater conductivity than CNT-COOH. The Warburg resistance which is mainly associated to psuedocapacitance is found to be greater for CNT-COOH/ZnO which is due to the faradaic properties of the ZnO nanoparticles [49–51].

Table 2 Fitting parameters as obtained for the samples

Sample code	*R*s (Ω)	*C* (F cm^{-2})	*R*ct (Ω)	*W* (Ω $s^{(1/2)}$)
CNT-COOH	43.63	8.36×10^{-6}	0.6128	0.0001808
CNT-COOH/ZnO	6.62	8.962×10^{-4}	0.06678	0.0005781

4 Conclusions

Acid functionalized carbon nanotubes and ZnO coated acid functionalized carbon nanotubes have been prepared using a microwave assisted technique. Both the samples have been extensively characterised and their electrochemical properties have been studied in details. A comparison has been made to analyse the effect of ZnO incorporation on the electrochemical efficacy of the sample. CNT-COOH/ZnO shows an enhanced specific capacitance of 628.88 F g^{-1} at 5 mV s^{-1} whereas CNT-COOH exhibits a specific capacitance of 311.1 F g^{-1} at 5 mV s^{-1}. Moreover, the sample also shows a good chronopotentiometric response coupled with a high cycling stability. The high electrochemical performance of CNT-COOH/ZnO indicates that it can be utilised for energy storage applications. Therefore, it can be concluded that the approach of composite formation can be very effective in elevating the electrochemical properties of materials which can be exploited greatly in the commercial aspect of developing electrochemical supercapacitors.

Acknowledgements We would like to thank the DST-FIST programme-2015 LEVEL 0 for providing us with the instrumentation facilities to carry out this research work. We are grateful to the Centre for Research in Science and Technology (CRIST), Stella Maris College, Chennai for helping us with the characterisation of the samples.

Declarations

Conflict of interest The authors declare that they have conflict of interest.

References

1. Kim BK, Sy S, Yu A, Zhang J (2015) Electrochemical supercapacitors for energy storage and conversion. Handb Clean Energy Syst. https://doi.org/10.1002/9781118991978.hces112
2. Yassine M, Fabris D (2017) Performance of commercially available supercapacitors. Energies. https://doi.org/10.3390/en10091340
3. Raza W, Ali F, Raza N et al (2018) Recent advancements in supercapacitor technology. Nano Energy 52:441–473. https://doi.org/10.1016/j.nanoen.2018.08.013
4. Gautham Prasad G, Shetty N, Thakur S et al (2019) Supercapacitor technology and its applications: a review. IOP Conf Ser Mater Sci Eng. https://doi.org/10.1088/1757-899X/561/1/012105
5. Miguel M, Nogueira T, Martins F (2017) Energy storage for renewable energy integration: the case of Madeira Island, Portugal. Energy Procedia 136:251–257. https://doi.org/10.1016/j.egypro.2017.10.277
6. Fisher RA, Watt MR, Jud Ready W (2013) Functionalized carbon nanotube supercapacitor electrodes: a review on pseudocapacitive materials. ECS J Solid State Sci Technol 2:M3170–M3177. https://doi.org/10.1149/2.017310jss
7. Demming A (2016) Supercapacitors empower sustainable energy storage. Nanotechnology. https://doi.org/10.1088/0957-4484/27/25/250201
8. Bakker MG, Frazier RM, Burkett S et al (2012) Perspectives on supercapacitors, pseudocapacitors and batteries. Nanomater Energy 1:136–158. https://doi.org/10.1680/nme.11.00007
9. Zhang Y, Feng H, Wu X et al (2009) Progress of electrochemical capacitor electrode materials: a review. Int J Hydrogen Energy 34:4889–4899. https://doi.org/10.1016/j.ijhydene.2009.04.005
10. Zhang Y, Mei H, Cao Y et al (2021) Recent advances and challenges of electrode materials for flexible supercapacitors. Coord Chem Rev 438:21390. https://doi.org/10.1016/j.ijhydene.2009.04.005
11. Kiamahalleh MV, Zein SHS, Najafpour G et al (2012) Multiwalled carbon nanotubes based nanocomposites for supercapacitors: a review of electrode materials. Nano. https://doi.org/10.1142/S1793292012300022
12. Conway BE (1999) Electrochemical supercapacitors scientific fundamentals and technological applications
13. Kamran U, Heo YJ, Lee JW, Park SJ (2019) Functionalized carbon materials for electronic devices: a review. Micromachines. https://doi.org/10.3390/mi10040234
14. Pan H, Li J, Feng YP (2010) Carbon nanotubes for supercapacitor. Nanoscale Res Lett 5:654–668. https://doi.org/10.1007/s11671-009-9508-2
15. Choi H, Yoon H (2015) Nanostructured electrode materials for electrochemical capacitor applications. Nanomaterials 5:906–936. https://doi.org/10.3390/nano5020906
16. Gul H, Shah AUHA, Krewer U, Bilal S (2020) Study on direct synthesis of energy efficient multifunctional polyaniline–graphene oxide nanocomposite and its application in aqueous symmetric supercapacitor devices. Nanomaterials. https://doi.org/10.3390/nano10010118
17. Pelinovskaya N, Bottero J, Masion A (2012) Encyclopedia of nanotechnology
18. Sasirekha C, Arumugam S, Muralidharan G (2018) Green synthesis of ZnO/carbon (ZnO/C) as an electrode material for symmetric supercapacitor devices. Appl Surf Sci 449:521–527. https://doi.org/10.1016/j.apsusc.2018.01.172
19. Simon R, Chakraborty S, Konikkara N, Mary NL (2020) Functionalized polystyrene maleic anhydride copolymer/ZnO nanocomposites for enhanced electrochemical performance. J Appl Polym Sci. https://doi.org/10.1002/app.48945
20. Chakraborty S, M AR, Mary NL, (2020) Biocompatible supercapacitor electrodes using green synthesised ZnO/Polymer nanocomposites for efficient energy storage applications. J Energy Storage. https://doi.org/10.1016/j.est.2020.101275
21. Li Y, Huang X, Zeng L et al (2019) A review of the electrical and mechanical properties of carbon nanofiller-reinforced polymer composites. J Mater Sci 54:1036–1076. https://doi.org/10.1007/s10853-018-3006-9
22. Flahaut E, Peigney A, Laurent C et al (2000) Carbon nanotube-metal-oxide nanocomposites: microstructure, electrical conductivity and mechanical properties. Acta Mater 48:3803–3812. https://doi.org/10.1016/S1359-6454(00)00147-6
23. Zhang Y, Chang C, rong, Jia X dong, et al (2020) Morphology-dependent NiMoO4/carbon composites for high performance supercapacitors. Inorg Chem Commun. https://doi.org/10.1016/j.inoche.2019.107631
24. Zhang Y, Chang C, rong, Jia X dong, et al (2020) Influence of metallic oxide on the morphology and enhanced supercapacitive performance of NiMoO4 electrode material. Inorg Chem Commun. https://doi.org/10.1016/j.inoche.2019.107697
25. Zhang Y, Mei HX, Gao HL et al (2020) Metal oxide modified (NH4) (Ni, Co)PO4·067H2O composite as high-performance

electrode materials for supercapacitors. Inorg Chem Commun 112:107696
26. Sadegh H, Shahryari-Ghoshekandi R, Agarwal S et al (2015) Microwave-assisted removal of malachite green by carboxylate functionalized multi-walled carbon nanotubes: kinetics and equilibrium study. J Mol Liq 206:151–158. https://doi.org/10.1016/j.molliq.2015.02.007
27. Khan J, Ilyas S, Akram B et al (2018) Zno/NiO coated multi-walled carbon nanotubes for textile dyes degradation. Arab J Chem 11:880–896. https://doi.org/10.1016/j.arabjc.2017.12.020
28. Chakraborty S, Mary NL (2020) A carbon nanotube reinforced functionalized styrene-maleic anhydride copolymer as an advanced electrode material for efficient energy storage applications. New J Chem 44:4406–4416. https://doi.org/10.1039/c9nj05978d
29. Chakraborty S, Farida JJ, Simon R et al (2020) Averrhoe carrambola fruit extract assisted green synthesis of zno nanoparticles for the photodegradation of congo red dye. Surf Interfaces 19:100488. https://doi.org/10.1016/j.surfin.2020.100488
30. Abdullah OG, Aziz SB, Omer KM, Salih YM (2015) Reducing the optical band gap of polyvinyl alcohol (PVA) based nanocomposite. J Mater Sci Mater Electron 26:5303–5309. https://doi.org/10.1007/s10854-015-3067-3
31. Mishra SK, Tripathi SN, Choudhary V, Gupta BD (2015) Surface plasmon resonance-based fiber optic methane gas sensor utilizing graphene-carbon nanotubes-poly (Methyl Methacrylate) hybrid nanocomposite. Plasmonics 10:1147–1157. https://doi.org/10.1007/s11468-015-9914-5
32. Chen CS, Chen XH, Yi B et al (2006) Zinc oxide nanoparticle decorated multi-walled carbon nanotubes and their optical properties. Acta Mater 54:5401–5407. https://doi.org/10.1016/j.actamat.2006.07.003
33. Malikov EY, Muradov MB, Akperov OH et al (2014) Synthesis and characterization of polyvinyl alcohol based multiwalled carbon nanotu be nanocomposites. Phys E Low Dimens Syst Nanostruct 61:129–134. https://doi.org/10.1016/j.physe.2014.03.026
34. Hong RY, Qian JZ, Cao JX (2006) Synthesis and characterization of PMMA grafted ZnO nanoparticles. Powder Technol 163:160–168. https://doi.org/10.1016/j.powtec.2006.01.015
35. de Menezes BRC, Ferreira FV, Silva BC et al (2018) Effects of octadecylamine functionalization of carbon nanotubes on dispersion, polarity, and mechanical properties of CNT/HDPE nanocomposites. J Mater Sci 53:14311–14327. https://doi.org/10.1007/s10853-018-2627-3
36. Silambarasan M, Saravanan S, Soga T (2015) Raman and photoluminescence studies of Ag and Fe-doped ZnO nanoparticles. Int J ChemTech Res 7:1644–1650
37. Jyothibasu JP, Chen MZ, Lee RH (2020) Polypyrrole/Carbon nanotube freestanding electrode with excellent electrochemical properties for high-performance all-solid-state supercapacitors. ACS Omega. https://doi.org/10.1021/acsomega.9b04029
38. Takassi MA, Zadehnazari A (2017) Green synthesis of salicylic acid-based poly (amide-imide) in ionic liquid and composite formation with multiwalled carbon nanotube. Polym Plast Technol Eng 56:1358–1365. https://doi.org/10.1080/03602559.2016.1275686
39. Tahermansouri H, Dehghan Z, Kiani F (2015) Phenol adsorption from aqueous solutions by functionalized multiwalled carbon nanotubes with a pyrazoline derivative in the presence of ultrasound. RSC Adv 5:44263–44273. https://doi.org/10.1039/c5ra02800k
40. Birch ME, Ruda-Eberenz TA, Chai M et al (2013) Properties that influence the specific surface areas of carbon nanotubes and nanofibers. Ann Occup Hyg 57:1148–1166. https://doi.org/10.1093/annhyg/met042
41. Norzilah AH, FakhruL-Razi A, Choong TSY, Chuah AL (2011) Surface modification effects on CNTs adsorption of methylene blue and phenol. J Nanomater. https://doi.org/10.1155/2011/495676
42. Chen Y, Liu C, Li F, Cheng HM (2006) Pore structures of multi-walled carbon nanotubes activated by air, CO2 and KOH. J Porous Mater 13:141–146. https://doi.org/10.1007/s10934-006-7017-6
43. Septiani NLW, Yuliarto B, Nugraha, Dipojono HK (2017) Multiwalled carbon nanotubes–zinc oxide nanocomposites as low temperature toluene gas sensor. Appl Phys A Mater Sci Process 123:0. https://doi.org/10.1007/s00339-017-0803-y
44. Zhang M, Li Q, Fang D et al (2015) NiO hierarchical hollow nanofibers as high-performance supercapacitor electrodes. RSC Adv 5:96205–96212. https://doi.org/10.1039/c5ra17011g
45. Wang G, Liang R, Liu L, Zhong B (2014) Improving the specific capacitance of carbon nanotubes-based supercapacitors by combining introducing functional groups on carbon nanotubes with using redox-active electrolyte. Electrochim Acta 115:183–188. https://doi.org/10.1016/j.electacta.2013.10.165
46. Inamuddin SN, Imran Ahamed M et al (2020) Green synthesis of ZnO nanoparticles decorated on polyindole functionalized-MCNTs and used as anode material for enzymatic biofuel cell applications. Sci Rep 10:1–10. https://doi.org/10.1038/s41598-020-61831-4
47. Balakrishna Pillai P, Kumar A, Song X, De Souza MM (2018) Diffusion-controlled faradaic charge storage in high-performance solid electrolyte-gated zinc oxide thin-film transistors. ACS Appl Mater Interfaces 10:9782–9791. https://doi.org/10.1021/acsami.7b14768
48. Song X, Chen Q, Shen E, Liu H (2020) N-Doped 3D hierarchical carbon from resorcinol-formaldehyde-melamine resin for high-performance supercapacitors. New J Chem 44:8638–8649. https://doi.org/10.1039/c9nj06415j
49. Mohan U, Gogoi P, Baruah SK (2017) Mixed ionic and electronic conductivity study of charge transfer complexes of some substituted pyridines with iodine monochloride (ICl) by AC impedance spectroscopy. Ionics 23:157–168. https://doi.org/10.1007/s11581-016-1794-y
50. Sivaraman P, Mishra SP, Potphode DD et al (2015) A supercapacitor based on longitudinal unzipping of multi-walled carbon nanotubes for high temperature application. RSC Adv 5:83546–83557. https://doi.org/10.1039/c5ra13136g
51. Kampouris DK, Ji X, Randviir EP, Banks CE (2015) A new approach for the improved interpretation of capacitance measurements for materials utilised in energy storage. RSC Adv 5:12782–12791. https://doi.org/10.1039/c4ra17132b